

## Visualization of collisional substructure in granular shock waves

John A. Perez,<sup>\*</sup> Samuel B. Kachuck, and Greg A. Voth<sup>†</sup>

*Department of Physics, Wesleyan University, Middletown, Connecticut 06459, USA<sup>‡</sup>*

(Received 1 July 2008; published 27 October 2008)

We study shock wave formation and propagation in an experimental vertically driven quasi-two-dimensional granular gas. We measure the moments of the single particle velocity distribution as a function of space and time. The space-time fields of the velocity moments show acoustic waves with a serrated substructure on the scale of a particle diameter. We show that this substructure is the result of collisional transport in which sequential collisions each transport momentum and energy by one particle diameter.

DOI: [10.1103/PhysRevE.78.041309](https://doi.org/10.1103/PhysRevE.78.041309)

PACS number(s): 45.70.-n

### I. INTRODUCTION

Vertically vibrated granular gasses are fluidized by acoustic waves that propagate upward through the system. This simple system produces a vast variety of fascinating phenomena ranging from size segregation [1] to pattern formation [2] and oscillons [3] to convection [4,5] and “Leidenfrost layers” [6,7].

Our interest in this paper is in the detailed structure of the shock waves that fluidize these systems. Several studies have explored these shock waves. Bougie *et al.* [8] performed a careful numerical study of a granular layer driven at fairly low frequency and found that solutions of hydrodynamic equations agree with molecular dynamics simulations on the shock positions, shape, and speed. Huang *et al.* [9] have experimentally measured the propagation of shock waves in a quasi-two-dimensional (2D) granular gas. NMR measurements of a 3D vertically vibrated granular gas show time resolved profiles of density and particle displacement [10,11]. Besides these studies, the extensive work on vertically vibrated granular materials has focused on time averaged properties [12–18].

There are four primary nondimensional parameters needed to define the motion of a sinusoidally vibrated granular layer [6]: (i) the normalized acceleration,  $\Gamma = \omega^2 A / g$ , where  $\omega$  is the angular frequency of the drive,  $A$  is the oscillation amplitude, and  $g$  is the gravitational acceleration; (ii) the number of layers of beads,  $N_y$ ; (iii) the ratio of oscillation amplitude to particle diameter,  $A^* = A / d$ , and (iv) the coefficient of velocity restitution,  $r$ . There are other factors such as the elastic moduli of the particles, friction coefficients, velocity dependence of the coefficient of restitution, and geometrical dimensions of the container that could be included also. However, these factors are less important, and factors like friction and velocity-dependent restitution are quite difficult to measure, so typically only the four primary parameters are specified. Three alternate combinations of the four parameters are worth mentioning separately. The dimensionless shaking strength,  $S = A^2 \omega^2 / g d = \Gamma A^*$ , gives the ratio

of the injected kinetic energy to the potential energy change from moving a bead by one diameter. The dimensionless frequency,  $\omega^* = \omega \sqrt{d/g} = \sqrt{\Gamma / A^*}$ , compares the time to fall one particle diameter to the driving period. The parameter  $X = N_y (1 - r)$  combines the number of layers supported by the gas with the inelastic energy loss [11,19].

This paper presents a series of measurements of the moments of the particle velocity in a granular gas under continuous vibration. We focus on the acoustic waves produced by the driving wall and find that they exhibit substructure on the scale of a particle diameter. These structures can be understood as the result of the two mechanisms for transport of momentum and energy in a granular gas. Kinetic (or streaming) transport occurs as particles carry their own momentum and energy along their trajectories. Collisional transport occurs when energy and momentum are transported across one particle diameter from one particle to another during a collision [20]. Kinetic transport is dominant at low densities while collisional transport is dominant at high densities. Kinetic transport occurs at the velocity of a typical particle, while collisional transport occurs at the velocity of sound inside a solid granular particle which is typically several orders of magnitude larger than particle velocities. In typical granular gasses, both modes of transport are important [21], and both contributions are usually included in calculations of stress and thermal conductivity from molecular dynamics simulations (see [22], for example).

### II. EXPERIMENT

The experiment consists of  $d = 3.175$  mm diameter borosilicate glass spheres constrained between glass plates separated by  $1.07d$ . Aluminum sidewalls confine the grains in a quasi-2D chamber with dimensions  $L_x = 29d$  by  $L_y = 21d$ . A photograph of the experimental chamber and a raw image is shown in Fig. 1. The same apparatus was used by Son *et al.* [23] to measure gravitational inelastic collapse of a granular gas.

The number of vertical layers  $N_y = Nd / L_x$ , where  $N$  is the total number of beads in the chamber, ranges from 2 to 20. The rigid chamber along with an accelerometer is directly attached to an LDS v450 electromechanical shaker from LDS Test and Measurement. The chamber is vertically vibrated at a frequency of  $f = \omega / 2\pi = 100$  Hz and amplitude of  $A = 0.87$  mm. From this we obtain the nondimensional pa-

<sup>\*</sup>Present address: Enterprise Risk Management, The Hartford, Simsbury, CT 06089, USA.

<sup>†</sup>gvoth@wesleyan.edu

<sup>‡</sup>URL: <http://gvoth.web.wesleyan.edu/lab.htm>

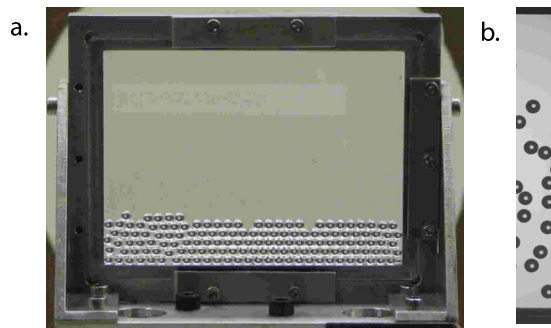


FIG. 1. (Color online) (a) Photograph of the apparatus containing  $N_y=5$  layers of spheres confined in a quasi-2D layer. (b) Raw image of a vertical strip with width  $3d$  in the center of the chamber.

rameters  $A^*=A/d=0.27$ ,  $\Gamma=35$ ,  $S=9.6$ , and  $\omega^*=11.3$ . Es-huis *et al.* [5,6] provide a comprehensive study of the phase diagram of a vertically vibrated quasi-2D granular system. We cannot compare directly because our experiment is at lower vibration amplitude, and hence higher frequency at fixed  $\Gamma$ , than they studied. However, extrapolation of their phase diagrams suggests that there should be gas states for small  $N_y$ , and density inversion (Leidenfrost states) at larger  $N_y$ , which is consistent with our observations. We do not observe any convection or undulations. We chose higher frequencies than most previous studies in order to obtain states where the shock waves are weaker in order to have a nearly time-independent initial state for studies of gravitational collapse [23]; but we find that the shock waves still show fascinating structure.

We attempted to quantify the coefficients of restitution,  $r$ , by measuring glass spheres impacting a glass plate, for which  $r=0.98$ , and glass spheres impacting an aluminum plate, for which  $r=0.92$ . Both of these show a slight decrease with increasing velocity. We have also measured sphere-sphere collisions in the chamber and found an average  $r$  in the range of 0.97, but the distribution is quite broad and extends well above 1, probably due to coupling between rotation and translation. If we estimate  $r=0.95$  as a typical value, then  $X$  ranges from 0.1 to 1 over the layer depths studied.

Images of the granular gas are captured at a rate of 3700 frames per second using a Basler A504k high speed camera. Preliminary measurements showed that the granular gas states are horizontally homogeneous away from the sidewalls, and so the system is statistically one dimensional. Accordingly, we imaged only a  $3d$  wide vertical strip in the center of the cell spanning the full height of the chamber using  $128 \times 1280$  pixels. This width was chosen as a compromise between the need to image several bead diameters while obtaining maximum frame rate. The chamber is backlit using a 750 W theater lamp and an opal diffusing glass with a circular aperture. As seen in Fig. 1, this produces a bright background on which the spheres appear dark with an image of the aperture near the center of each sphere. A surprisingly bright and uniform background illumination can be achieved by simply placing the diffusing glass parallel to the viewing window and the theater lamp at an oblique angle to the diffusing glass.

The data acquisition process is automated by means of custom Labview software which generates the sinusoidal drive wave form for the shaker and synchronously triggers the camera. The 3700 Hz camera frequency produces 37 images per period. For each density we imaged approximately 16 000 statistically identical drive cycles with 576 000 images and almost 80 Gb of data. The positions of particle centers were extracted from the images with an accuracy of better than  $1/20$  of a pixel. An image of a sphere spans 40 pixels so the position accuracy is  $1/800$  of a particle diameter or  $4.0 \mu\text{m}$ . IDL particle tracking codes [24] were used to track particles through sequential frames and then velocities were computed by simple differences in position over a time step.

Since the driving wall moves periodically in time, we can ensemble average over different drive cycles and obtain a high resolution sampling of the single particle distribution function,  $f(\vec{r}, \vec{v}, t)$ . We focus on measurements of four moments of the vertical velocity. The zeroth moment gives the number density and the first moment gives the mean velocity. The variance and skewness are determined by the second and third moments of the deviation from the mean.

The statistics vary only in the vertical direction since we measure far away from the sidewalls, so we calculate the velocity moments as a function of vertical position and time. The camera frame rate provides the temporal bin size as  $1/37$  of a period. The vertical coordinate is divided into 400 bins, or about one-tenth of a particle diameter per bin. Earlier studies have chosen to make their bin size equal to the particle size [8,9]. This is an appropriate choice in order to obtain fields that can be compared with continuum hydrodynamic models, but it smooths out any particle scale substructure in the measurements.

One important consideration when using bins smaller than the particle size is to determine which bin to register a particle velocity in. We have chosen the bin containing the particle center. This means that samples will only occur in bins that are at least one radius from the walls. Other protocols, such as registering each particle's velocity with all positions inside the sphere or with all positions in the sphere's Voronoi volume are possible. These give smoother fields and are arguably appropriate when comparing with hydrodynamic models. However, they inherently smooth out the correlations that exist in the particle velocities. Although it takes much more data to produce smooth fields of velocity moments registered by the particle center, this method allows us to observe particle scale correlations.

### III. RESULTS

Figure 2 shows the vertical velocity variance,  $\langle(v_y - \langle v_y \rangle)^2\rangle$ , or granular temperature, as a function of vertical position and time. The most obvious feature is the high temperature acoustic waves that propagate in from the top and bottom of the chamber when the wall is moving into the gas. A more careful look at the high temperature wave created by the lower wall in Fig. 2 reveals a serrated substructure to the wave. The vertical spacing between the serrations is one particle diameter, and each serration looks like a dif-

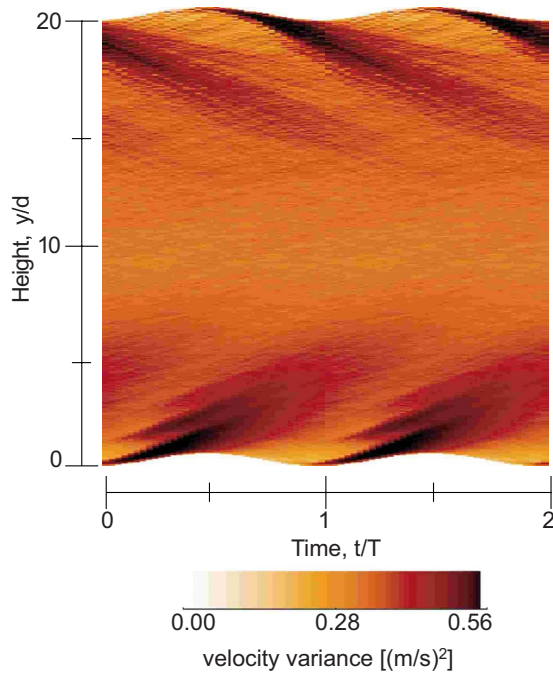


FIG. 2. (Color online) Vertical velocity variance for  $N_y=5$  layers. The phase averaged data are repeated over two periods of the sinusoidal driving to show all the structure. Height equal to zero is defined as the lowest position of a particle center, which is half a particle diameter above the bottom wall.

ferent wave starting at a different height in the chamber. Note that the high temperature shocks moving downward from the top wall do not have the same serrated substructure. We will see that this is caused by the much lower density near the top boundary.

Figure 3 shows four moments of the vertical velocity as a function of space and time. The density field, Fig. 3(a), shows the expected decrease of density with height due to gravity, but the signatures of the serrations are very weak. The higher moments of the velocity show the serrations more clearly. The high temperature regions are also regions of upward mean velocity and positive velocity skewness. Moving from Fig. 3(a) to Fig. 3(d), the serrations appear to extend farther up into the chamber. For the skewness in Fig. 3(d), the fourth serration is barely visible.

**A. Collisional transport**

The structures in the acoustic waves are the result of collisional transport. Energy and momentum are transported by particles as they move, but when a collision occurs, the transport speed changes from the particle velocity to the speed of sound in glass, which is four orders of magnitude larger. As a result, the most rapid transport of energy into the gas occurs by sequential collisions. The first serration consists of particles that recently collided with the lower boundary. The second serration is from particles that collided with a particle that had recently collided with the lower boundary, and so on.

Figure 4 visualizes this process by superimposing three measured particle trajectories on the serrations in the tem-

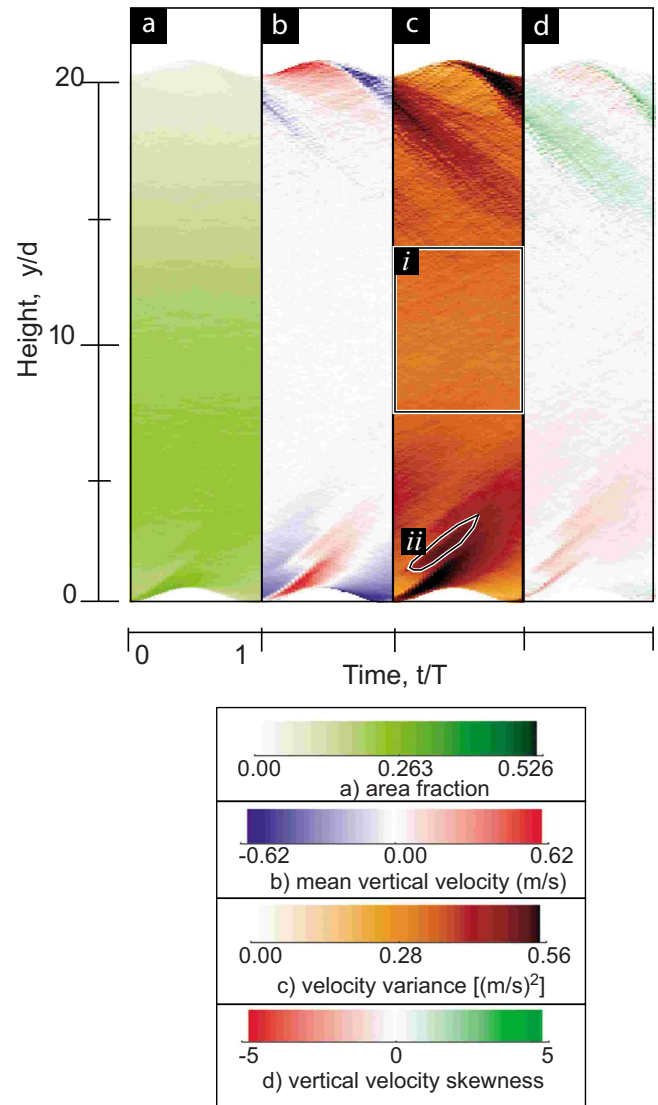


FIG. 3. (Color online) Four moments of the vertical velocity, each over one oscillation cycle.  $N_y=5$ . (a) Density or zeroth moment of the velocity, (b) Mean velocity,  $\langle v_y \rangle$ , (c) velocity variance,  $\langle (v_y - \langle v_y \rangle)^2 \rangle$ , and (d) velocity skewness,  $\langle (v_y - \langle v_y \rangle)^3 \rangle / \langle (v_y - \langle v_y \rangle)^2 \rangle^{3/2}$ . In (c) the regions (i) and (ii) indicate regions whose velocity distribution is shown in Fig. 5.

perature field. First a downward moving particle encounters the upward moving bottom wall at time  $t_1$ . This collision sends the first particle on a short-lived and rapid upward ballistic flight which terminates in a collision with a second downward moving particle at time  $t_2$ . The collision scatters the first particle downward and transfers most of its energy to the upward motion of the second particle. Between times  $t_2$  and  $t_3$ , the second particle contributes to the second serration. The collision transports the energy to a position that cannot be reached by particles that recently collided with the lower boundary, so the second serration is separated from the first by one particle diameter. The second particle then repeats this sequence when it scatters off a third particle at time  $t_3$  to form the third serration.

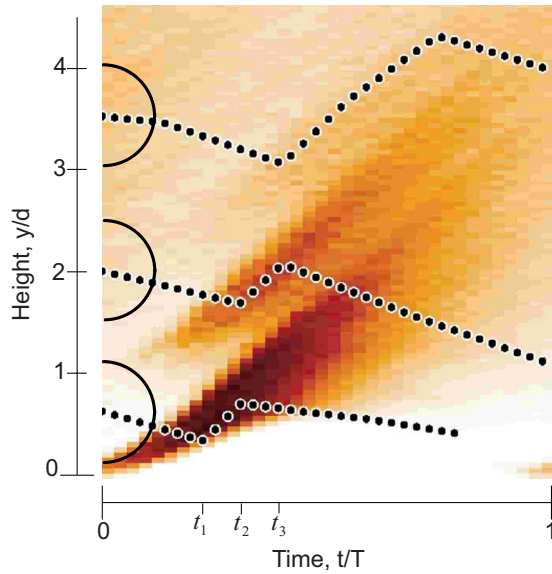


FIG. 4. (Color online) Three measured particle trajectories superimposed on the granular temperature field. The circles at the left indicate the size of the particles. Black dots indicate the position of the center of the particles. Collisions at times  $t_1$ ,  $t_2$ , and  $t_3$  are responsible for creating the substructure in the acoustic wave.

### B. Velocity distributions

The probability density function (PDF) of vertical velocity is shown in Fig. 5. A larger space-time region is needed to get enough samples to resolve the PDF, and the regions selected have been marked in Fig. 3(c). The distribution including all samples shows a slight positive skewness. When only samples from the nearly time independent region near the center of the chamber are included, the skewness is smaller but still visible. When only samples in the region of the second serration are included, the distribution is bimodal. The bimodal distribution is far from the Maxwell-Boltzmann distribution of a gas in equilibrium, but is typical of shock waves. The success of continuum hydrodynamic models in describing wave propagation in this flow [8] despite the

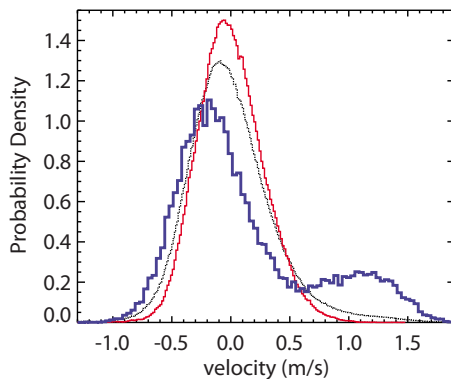


FIG. 5. (Color online) Velocity distributions. The dotted line includes samples from the entire chamber. The solid line includes samples in region (i) from Fig. 3(c). The bold line includes only samples from the second serration, region (ii) from Fig. 3(c). Parameters are the same as Figs. 2 and 3.

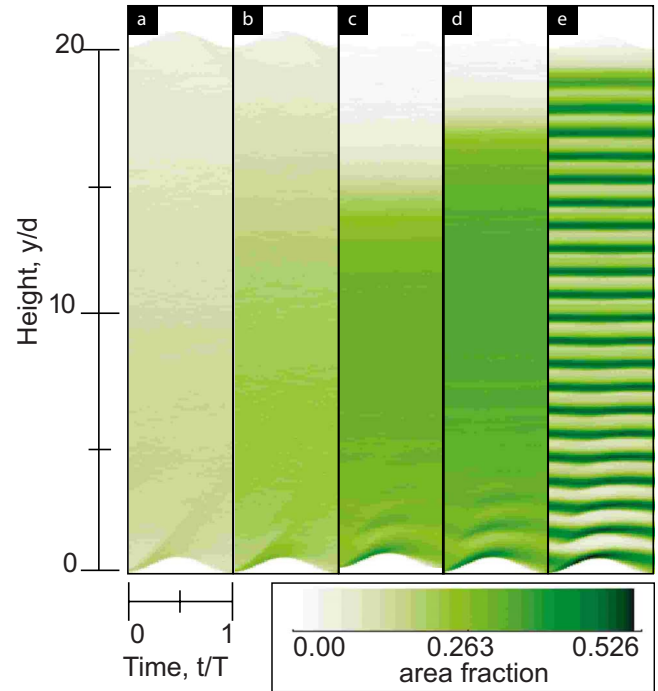


FIG. 6. (Color online) Area fraction fields for five experiments, each with a different number of layers. A typical area fraction  $\bar{\phi}$  is defined by the averaging the density across the high density plateau in each data set. (a)  $N_y=2$ ,  $\bar{\phi}=0.11$ ; (b)  $N_y=5$ ,  $\bar{\phi}=0.28$ ; (c)  $N_y=10$ ,  $\bar{\phi}=0.54$ ; (d)  $N_y=15$ ,  $\bar{\phi}=0.67$ ; and (e)  $N_y=20$ ,  $\bar{\phi}=0.78$ . Note the crystallization that occurs between (d) and (e).

highly nonequilibrium velocity distributions is remarkable.

We confirmed the collisional interpretation of the serrations by looking at raw image sequences of high velocity particles in the third serration. The velocity PDF for the region of the third serration is bimodal like the PDF from the second serration, although the positive velocity peak is smaller in the third serration. We selected particles with velocities in the positive peak and viewed the sequence of raw images for these particles. In every case, we saw a sequence of three collisions similar to those shown in Fig. 4.

### C. Dependence on number of granular layers

Figure 6 shows the density fields for five different experiments at fixed vibration frequency and fixed amplitude with the number of layers of particles in the chamber ranging from  $N_y$  of 2 to 20. The most dramatic change in the density field is between 15 and 20 layers where the system crystallizes. The average area fraction taken over the plateau of nearly uniform density ranges from 0.11 to 0.78. Crystallization occurs between area fractions of 0.67 and 0.78, consistent with the crystallization density of 2D hard spheres at 0.716 [25]. The density near the top of the chamber initially decreases as  $N_y$  increases. This can be understood as increased hydrostatic pressure increasing the collision frequency and hence energy dissipation rate. Alternately, increasing  $N_y$  increases  $X$  implying less fluidization. For the higher number of particles, the particles fill more of the chamber, and so the density near the top increases again.

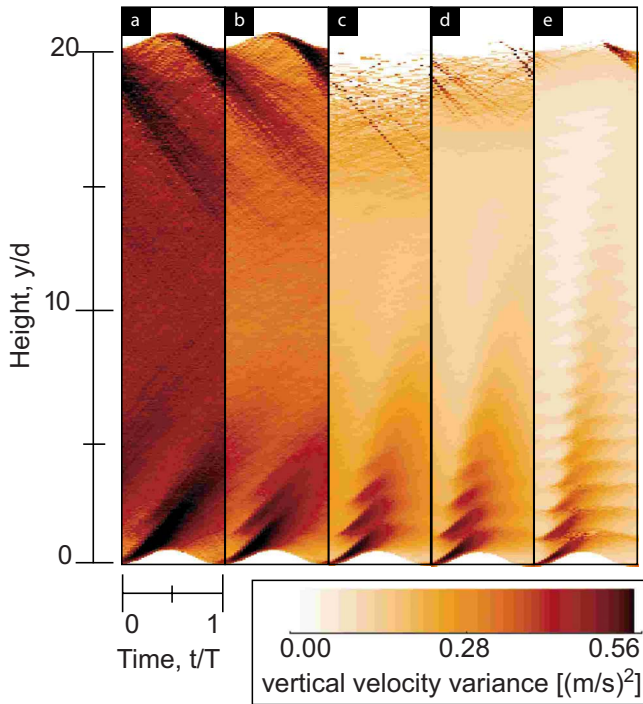


FIG. 7. (Color online) Vertical velocity variance field (temperature) for the same five data sets as Fig. 6.

The shock waves are barely visible in the density fields. In Figs. 6(c) and 6(d), a weak collisional substructure in the shock waves can be seen. The density field does not show the collisional substructure as clearly because it is not formed by a simple layering or crystallization of the particles. Even without any ordering of the particles, a collision will transmit energy faster than the particle velocity, and so a narrow shock wave will form collisional substructure in the temperature field, but it will be much less prominent in the density field.

Figure 7 shows the temperature field for several layer depths. At an area fraction of 0.11 [Fig. 7(a)], the second serration is already visible. As the density increases, the collisional substructure extends farther into the chamber. Interestingly, the signature of crystallization in the temperature field is primarily that the collisional substructure of the shock extends through the entire sample. Note that the temperature field for the crystallized state has a particle scale structure that extends through the entire period rather than decaying after half a period as it does in the disordered states of Figs. 7(a)–7(d).

Figure 8 shows the horizontal velocity variance, or horizontal temperature, for the same experiments as Fig. 7. In the horizontal temperature field, the collisional substructure is still visible although it is less well-defined. Because the vibration only couples directly into the vertical component, the shock waves in the horizontal temperature are significantly weaker. Note particularly that the first serration is weaker than the second because the bottom wall is flat and does not impart any horizontal energy. Only after an oblique collision does significant horizontal temperature appear. Additionally, when an oblique collision does create significant horizontal velocity, it also ends the upward sequence of collisions, and

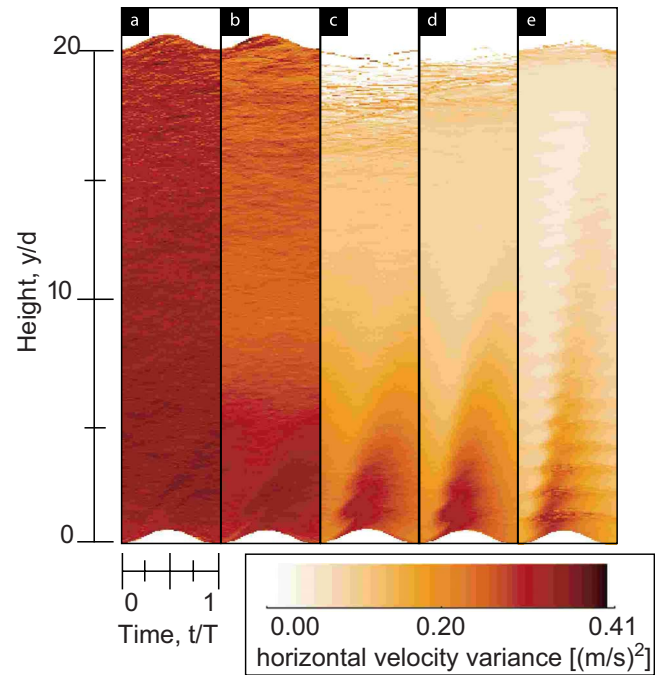


FIG. 8. (Color online) Horizontal velocity variance field (temperature) for the same five data sets as Fig. 6.

so it is expected that the horizontal temperature has less well-defined collisional substructure in the shock waves.

#### D. Discussion

The collisional substructure in these waves is the result of the nonlocal interaction involved in collisions. If we describe the system using granular coordinates which ignore the internal degrees of freedom of the particles, then a collision instantaneously transports momentum by one particle diameter. The particles actually interact by acoustic waves traveling through the solid material and so the interaction is local; however, most research on granular materials is guided by the goal of developing models in granular coordinates that parametrize the effects of internal degrees of freedom. In these granular models, collisions are unavoidably nonlocal. Continuum granular descriptions are often applied at scales down to less than one particle diameter [8,26]. This works when molecular chaos removes any correlations between positions and velocities at the particle scale. However, in our experiment, the particles that receive large velocity from collisions with the flat bottom plate are spread over a vertical range of less than one particle diameter. This means that their positions and velocities are highly correlated. The nonlocal interactions during collisions then allow the position-velocity correlations to extend well into the chamber and produce a complex pattern of position-velocity correlations that appear as the serrated collisional substructure.

The collisional substructure can also be viewed as a signature in the ensemble averaged fields of the collisional stress chains studied in [27]. This work was on flows at higher density, but our measurements show that even at lower densities, collisional transport can still create correla-

tions between position and velocity that extend over several particle diameters across a granular gas.

#### IV. CONCLUSIONS

Experimental measurements of the moments of the velocity in a vertically vibrated granular gas reveal that the acoustic waves that propagate through the gas have substructure on the scale of a particle diameter. Our primary contribution in this work is the visualization of this substructure and explanation in terms of a sequence of collisions which each transport momentum and energy by a particle diameter. The distributions of vertical velocity show positive skewness throughout the system with a bimodal distribution in the

shock waves. As the number of layers in the chamber is increased, the collisional substructure extends farther into the chamber. These measurements highlight the complex correlations between position and velocity that exist in granular gases.

#### ACKNOWLEDGMENTS

This work was supported by Wesleyan University, the Alfred P. Sloan Foundation, and NSF Grant No. DMR-0547712. We appreciate helpful discussions with Mark Shattuck. Wesleyan undergraduate Takanori Nagatomo performed preliminary explorations that led to these experiments.

- 
- [1] A. Kudrolli, *Rep. Prog. Phys.* **67**, 209 (2004).
  - [2] F. Melo, P. Umbanhowar, and H. L. Swinney, *Phys. Rev. Lett.* **72**, 172 (1994).
  - [3] P. B. Umbanhowar, F. Melo, and H. L. Swinney, *Nature (London)* **382**, 793 (1996).
  - [4] R. Ramirez, D. Risso, and P. Cordero, *Phys. Rev. Lett.* **85**, 1230 (2000).
  - [5] P. Eshuis, K. van der Weele, D. van der Meer, R. Bos, and D. Lohse, *Phys. Fluids* **19**, 123301 (2007).
  - [6] P. Eshuis, K. van der Weele, D. van der Meer, and D. Lohse, *Phys. Rev. Lett.* **95**, 258001 (2005).
  - [7] B. Meerson, T. Poschel, and Y. Bromberg, *Phys. Rev. Lett.* **91**, 024301 (2003).
  - [8] J. Bougie, SungJoon Moon, J. B. Swift, and H. L. Swinney, *Phys. Rev. E* **66**, 051301 (2002).
  - [9] K. Huang, G. Miao, P. Zhang, Y. Yun, and R. Wei, *Phys. Rev. E* **73**, 041302 (2006).
  - [10] X. Y. Yang, C. Huan, D. Candela, R. W. Mair, and R. L. Walsworth, *Phys. Rev. Lett.* **88**, 044301 (2002).
  - [11] C. Huan, X. Yang, D. Candela, R. W. Mair, and R. L. Walsworth, *Phys. Rev. E* **69**, 041302 (2004).
  - [12] S. Warr, J. M. Huntley, and G. T. H. Jacques, *Phys. Rev. E* **52**, 5583 (1995).
  - [13] F. Rouyer and N. Menon, *Phys. Rev. Lett.* **85**, 3676 (2000).
  - [14] K. Feitosa and N. Menon, *Phys. Rev. Lett.* **88**, 198301 (2002).
  - [15] R. D. Wildman and J. M. Huntley, *Phys. Fluids* **15**, 3090 (2003).
  - [16] K. Feitosa and N. Menon, *Phys. Rev. Lett.* **92**, 164301 (2004).
  - [17] S. J. Moon, J. B. Swift, and H. L. Swinney, *Phys. Rev. E* **69**, 011301 (2004).
  - [18] H. Viswanathan, R. Wildman, J. Huntley, and T. Martin, *Phys. Fluids* **18**, 113302 (2006).
  - [19] S. Luding, E. Clément, A. Blumen, J. Rajchenbach, and J. Duran, *Phys. Rev. E* **49**, 1634 (1994).
  - [20] C. S. Campbell and A. Gong, *J. Fluid Mech.* **164**, 107 (1986).
  - [21] C. S. Campbell, *Annu. Rev. Fluid Mech.* **22**, 57 (1990).
  - [22] C. Hrenya, J. Galvin, and R. Wildman, *J. Fluid Mech.* **598**, 429 (2008).
  - [23] R. Son, J. A. Perez, and G. A. Voth, *Phys. Rev. E* **78**, 041302 (2008).
  - [24] <http://www.physics.emory.edu/weeks/idl/>
  - [25] P. M. Reis, R. A. Ingale, and M. D. Shattuck, *Phys. Rev. Lett.* **96**, 258001 (2006).
  - [26] E. C. Rericha, C. Bizon, M. D. Shattuck, and H. L. Swinney, *Phys. Rev. Lett.* **88**, 014302 (2001).
  - [27] A. Ferguson and B. Chakraborty, *Phys. Rev. E* **73**, 011303 (2006).